12th International Conference on Ground Penetrating Radar, June 16-19, 2008, Birmingham, UK

Comparison of GPR Sensor Types for Landmine Detection and Classification

L. Capineri[1], S. Ivashov[2], T. Bechtel[3], A. Zhuravlev[2], P. Falorni[1], C. Windsor[4], G. Borgioli[1], I. Vasiliev[2], and A. Sheyko[2]

[1]University of Florence, Italy; [2] Bauman Moscow Technical University, Russia; [3]University of Pennsylvania, USA; [4]East Hagbourne, UK

capineri@ieee.org, sivashov@rslab.ru, bechtelt@sas.upenn.edu, azhuravlev@rslab.ru, pfalorni@hotmail.com, colin.windsor@ukaea.org.uk, giovanni.borgioli@unifi.it, ivasiliev@rslab.ru

***Abstract* - An effective detector for use in humanitarian de-mining must respond to metal and non-metal mines; reliably discriminate mines from clutter and decoys with a low rate of false-positives; discriminate amongst differing mine types; be lightweight; and be affordable. To address these sometimes competing specifications, we have evaluated an innovative, multi-channel, continuous-wave, holographic radar (RASCAN) and high resolution metal detector coil (MetalScan), developed at Bauman Moscow Technical University, Russia. The sensors in this system were used to image landmine simulants of various realistic construction, as well as clutter objects, in an outdoor test bed. RASCAN and MetalScan images were compared to matching images from a commercially-available StructureScan impulse radar.**

***Keywords* – holographic subsurface radar, impulse radar, metal detector, humanitarian demining.**

I. INTRODUCTION

War has been waged somewhere on the Earth for nearly all of human history [1]. Modern wars are often characterized by the widespread use anti-personnel and anti-tank landmines. Consequently, as of 2006, there are 78 countries with varying degrees of landmine infestation [2], with approximately ¼ of these being severely affected (e.g. Afghanistan, Iraq, Croatia, Egypt, Cambodia, Angola, Mozambique…) [3]. As many as 66 percent of the world's poorest people (subsistence farmers) live with the daily threat of landmines. This results in 15 to 20 thousand casualties per year, with the vast majority being civilians (particularly children) since military personnel are trained and equipped to avoid landmines. Beyond the obvious casualties, mine-related elimination of vast tracts of arable land from agricultural production, and the mining of water supplies result in up to 100 percent dependence on international food aid in some regions.

Currently, in the ground, and in the arsenals of various governments and armed groups, there are approximately 155 million mines of about 600 different type. The different landmine types have differing purpose (i.e. anti-personnel vs. anti-tank); explosive content; projectiles or shrapnel; triggering or fuzing devices; anti-tampering devices; and housing (e.g. metal, plastic, or ceramic) [4].

On average, the cost to produce a single mine is $3 USD (anti-personnel) to $75 USD (anti-tank), and they can be laid quickly in great quantities by unskilled personnel. In contrast, removal must be done by highly skilled personnel, and may cost, on average, $300 to $500 USD per mine. Even with highly trained deminers, UN statistics indicate a loss of one or two deminers per 1000 mines removed [5].

Despite the 1998 "Ottawa Treaty", the limitations of current funding, methods and devices, coupled with deployment of landmines by non-signatories to the treaty as well as non-government armed groups, has led to an increase in the number of landmines in the ground worldwide. Although considerable effort and creativity have gone into development of devices for demining (see, e.g. [6], [7], [8]), no single system yet meets the (admittedly subjective) criteria for the "ideal" humanitarian demining system, namely:

1. low cost construction (to be affordable in war-ravaged countries)
2. easy transportation (for deployment in remote or rugged locales)
3. possibility of operation and interpretation by non-experts (to facilitate local performance and control of demining operations)
4. rapid deployment in emergencies (e.g. to clear important fields at critical points in the planting/harvest cycle)
5. high probability of detection for landmines (so landmines are not inadvertently left in the ground)
6. low false alarm rate (so that scant resources are spent removing mines and not clutter)
7. identification of landmine type (so that mines can be removed more safely, and cost-effectively), and
8. no degradation in performance in the rugged conditions of actual minefields.

Significant work, and attendant progress, have been realized in adapting Ground Penetrating Radar (GPR) [9] for landmine detection. Examples include the "Energy Focusing Ground Penetrating Radar" or EFGPR [10], the combined GPR and metal detector "Handheld Standoff Mine Detection System" or HSTAMIDS [11] and MINEHOUND [12], and the combined GPR, metal detector and infrared "Light Ordnance detection by Teleoperated Unmanned System" or LOTUS [13] – amongst others. While all of these, and other systems not cited, satisfy some, or even most, of the criteria above, none satisfy all.

a)

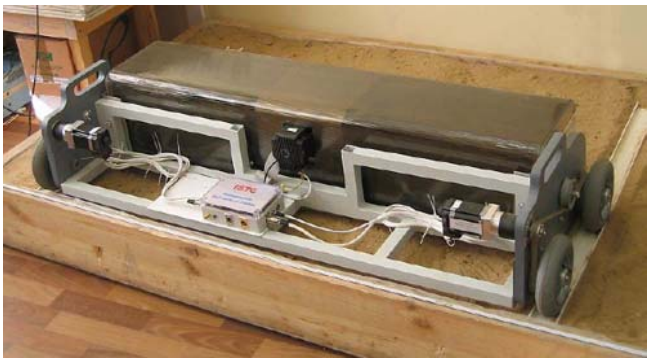

b)

Figure 1. Prototype MiRascan remote-control mine detector with coincident holographic radar and metal detector head (a), and the ISTC electromechanical scanner (b).

Beginning in the late 1980's, the staff of the Remote Sensing Laboratory (RSL) of Bauman Moscow Technical University undertook the development of microwave imaging devices for landmines, leading to the MiRascan combined GPR and metal detector system [14]. In MiRascan, a single scanning head contains a continuous-wave holographic radar antenna, and an induction metal detector coil. The radar has five discrete operational frequencies in the range of 1.5 - 2.0 GHz and transmits un-modulated signals at each frequency. Signals reflected by buried objects are received in two polarizations. Details of the theory and specifications of this type of radar are presented elsewhere in this volume [15]. The induction loop of the metal detector is located on the face of the radar antenna to ensure precise spatial coincidence of radar and metal detector image pixels. The operating frequency of the metal detector is 2 MHz, and the diameter of the induction coil is 120 mm. To maintain light weight and low cost, a single scanning head is used. This head is automatically swept back-and-forth as the system advances under remote control. Real-time metal detector and holographic subsurface radar images are transmitted to a computer monitor through a 15m umbilical control and data cable. An early mock-up of the MiRascan system is shown in Fig. 1-a. A recent fully operational version of this sensor system, developed under ISTC Project #2541, is shown in Fig. 1-b. Note that this platform is designed specifically for sounding of structures, and requires modification and further development for rugged or vegetated minefields.

The MiRascan and ISTC systems are lightweight, and readily transportable. The images are produced in real-time, with no required post-processing (e.g. migration), and as will be shown below, can be interpreted by unskilled personnel. The cost for the scanning head at the heart of the system is approximately $5000 USD. Thus, this system has the potential to meet many of the important criteria for a humanitarian demining system.

The purpose of this study was to perform simple field testing to determine whether the holographic radar and metal detector sensors of the type used in MiRascan could discriminate mines from clutter, and could provide images that would discriminate between different types of mine. In addition, having at our disposal an impulse radar with a center frequency similar (but not identical) to the holographic radar, we wished to compare impulse radar and holographic radar images of the test targets.

a)

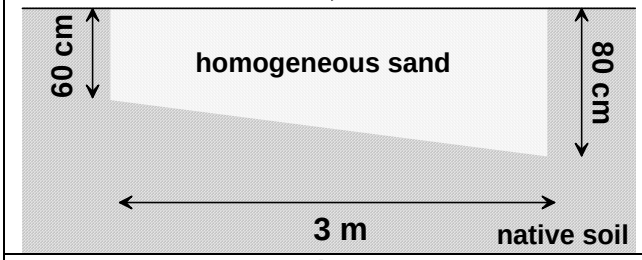

b)

Figure 2. Cross-section (a), and photo (b) of the University of Florence test bed.

II. TESTING SETUP

Testing was performed in a bed constructed by the University of Florence in 2004. The bed is 3m by 3m in plan, with a sloping base at 60 to 80cm to provide drainage, and minimize basal reflections (Fig. 2). The bed is filled with homogeneous sand that was slightly moist at the time of the testing.

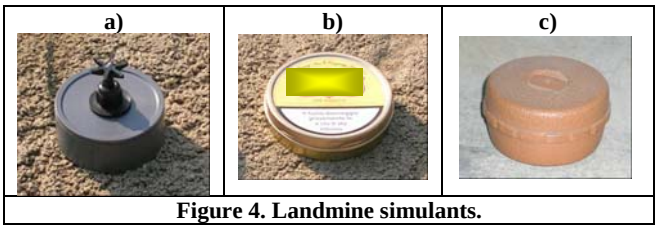

Figure 4. Landmine simulants.

Four landmine simulants were buried at shallow depth in the test bed. These included:

1. A PMA-2 simulant mine furnished by C. King Associates Ltd. (see Fig. 4-a), which reproduces the real PMA-2 anti-personnel landmine with diameter=6.9cm. The real PMA-2 mine contains 100.45g of Trotyl and a Tetryl booster pellet. This PMA-2 simulant is filled with RTV 3110 which has a dielectric constant similar to the actual explosives.
2. Two cylindrical, metallic pipe tobacco tins (Fig. 4-b) with diameter=10.5cm and height=2.5cm. This simulant is air-filled, but being metal, the filling is not important for radar imaging.
3. A cylindrical plastic case with diameter=10.5cm, and height=5.5cm, also air-filled with no metallic content (Fig. 4-c).

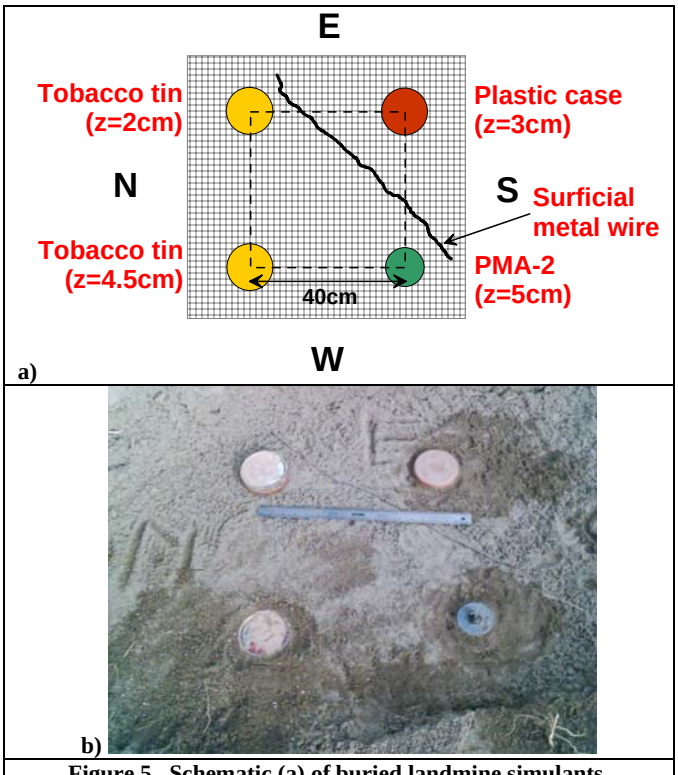

Figure 5. Schematic (a) of buried landmine simulants, and photo (b) of same.

These targets were placed in a shallow excavation in the pattern depicted in Fig. 5. Following backfilling, the target depths determined by probing. In addition to the landmine simulants, a strand of rusty steel wire was placed across the bed both to act as clutter, and to provide a feature to confirm image orientations (since the targets were cylindrical and in a symmetric pattern).

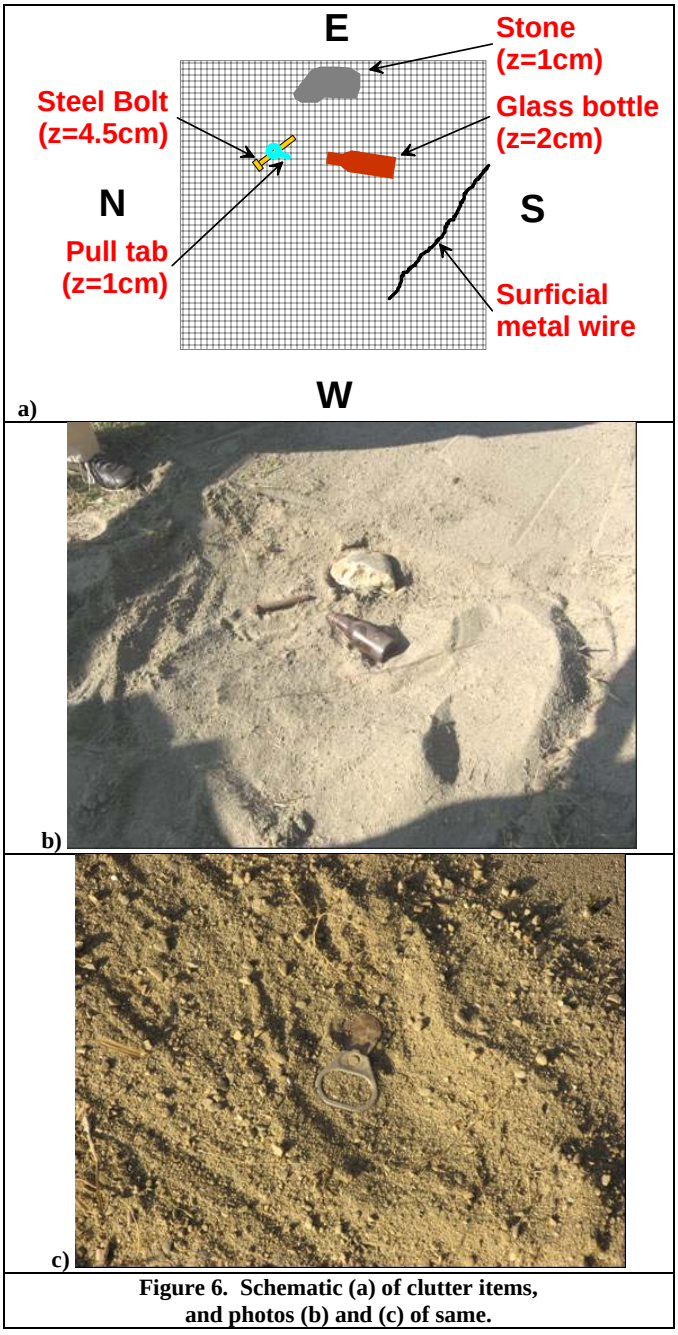

Figure 6. Schematic (a) of clutter items, and photos (b) and (c) of same.

Following scanning (as described below), the landmine simulants were removed, and clutter objects typical of those that might be found in a war zone were buried in the test bed. These clutter items included:

1. A glass bottle at a depth of 2cm,
2. A stone at 1cm,

3. An iron bolt at 4.5cm,
4. A metal wire on the surface,
5. An aluminum pull tab from a soda can at less than 1cm.

The clutter items are depicted in Fig. 6 prior to backfilling. The pull tab was placed in the bed when backfilling was nearly complete, and was inadvertently located directly above the bolt, leading to interesting images as described below

III. SUBSURFACE SCANNING

The landmine simulant, and clutter test beds were scanned using three instruments:

1. A RASCAN 4/4000 holographic radar built by the Remote Sensing laboratory of Bauman Moscow Technical University,
2. A MetalScan imaging induction metal detector, also by Bauman,
3. A GSSI StructureScan impulse radar.

The characteristics of these three sensors are summarized in Table 1. The first two devices were chosen to mimic the sensors in the prototype MiRascan device. The RASCAN 4/4000, with five discrete transmission frequencies between 3.6 and 4.0 GHz, is higher frequency than the actual MiRascan sensor, but operates on exactly the same principles and software. The MetalScan sensor is the same as the metal detector in the MiRascan device, but is not built into the radar antenna.

Because the RASCAN and MetalScan heads were not integrated as in the MiRascan device, scanning with each was performed on a ruled mat (a GSSI 3-D data collection pad), made of a synthetic material transparent to radar, anchored to the test bed to ensure coincidence of images. By using this mat as a template, all radar and metal detector images in this report are nearly coincident, with plan-view dimensions of 60cm by 60cm.

The third device, a GSSI StructureScan was chosen as the highest frequency impulse radar available to the authors at the time of testing. While there is overlap of the UWB signal waveband of this device with the five RASCAN 4/4000 frequencies, the center frequency of the UWB StructureScan impulse radar (1.5 GHz) was lower than any of the discrete RASCAN frequencies. However, the purpose of the testing was not to perform any type of head-to-head competition – particularly since none of the devices used in this study are designed specifically for landmine identification. Instead, the purpose was to demonstrate fundamental differences in the capabilities of the different types of devices by using each to scan the test bed in quick succession, thus ensuring identical targets and conditions (e.g. in a manner similar to previous impulse radar and metal detector comparisons by others [16]).

Scanning was performed by anchoring the data collection pad to the test bed with wooden stakes through holes in each corner, and then scanning, with each of the three devices, the area defined by the mat. For MetalScan and RASCAN, scans were performed along horizontal (E-W) grid lines at one centimeter intervals. For StructureScan, scanning was performed bi-directionally along an orthogonal grid of lines, at the 5 centimeter intervals printed on the data collection pad.

For MetalScan and RASCAN, plan-view images are compiled in real time, raster-by-raster, in RSL's MultiScan Software, as data collection proceeds. For StructureScan, data are collected as cross-sectional B-scan profiles, and then downloaded to a field PC for migration, and compilation into a 3-D block model using the StructureScan module of GSSI's RADAN software. The migration and compilation in RADAN is fully automated except for the selection of pulse velocity/dielectric constant for migration of the raw B-scan data. For this study, migration velocity was selected by trial-and-error iterations to find the velocity that best reduced parabolic B-scan reflection patterns to point targets.

The results of the MetalScan, RASCAN, and StructureScan imaging of the landmine test bed are depicted in Fig. 7. Note that while the MetalScan image is a complete representation of the data from this device, a single hardcopy image cannot provide all of the information revealed by either the RASCAN or StructureScan devices.

Table 1. Characteristics of Sensors

	MetalScan	**RASCAN**	**StructureScan**
Nominal Parameters			
Frequency spectrum:	2MHz induction	3.6, 3.7, 3.8, 3.8 and 4.0 GHz	UWB with 1.5GHz center
Penetration depth:	5 cm	1-2 λ	up to 10λ
Resolution at shallow depths in image plane:	3 cm	0.25 λ	> λ
Imaging Capabilities	Direct from recorded signal	Direct from recorded signal	Indirect (requires migration and stacking of B-scans)
Target depth measurement:	None	None	Direct from time-of-flight
Ease of adaptation to regulatory norms:	Simple	Simple	Difficult
Relative Cost:	Low	Low	High

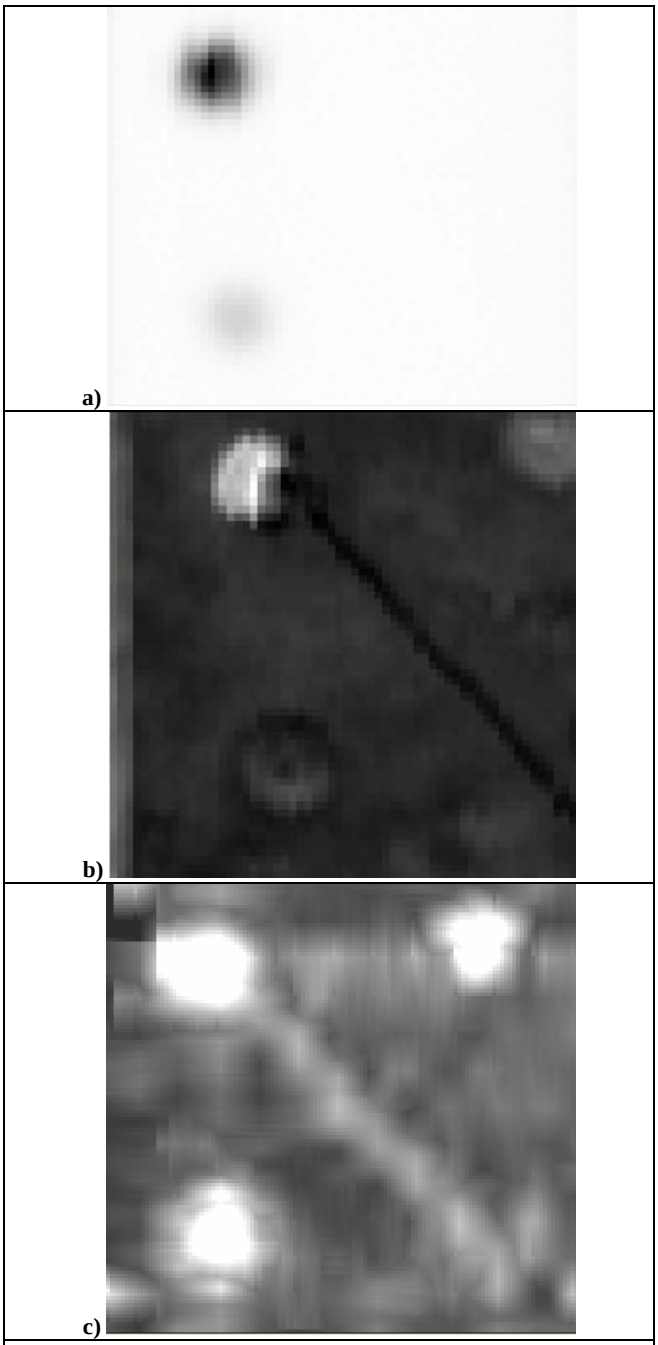

Figure 7. Semi-coincident MetalScan (a), RASCAN (b), and StructureScan (c) images (60cm by 60cm) of landmine simulants.

RASCAN produces ten simultaneous images at five frequencies for each of two different receiver polarizations (Fig. 8). As Fig. 8 shows, certain frequencies and/or polarizations provide clearer images due to greater phase differences – which cannot be predicted a-priori. The MultiScan software addresses this by providing a utility to construct a video in which the ten images smoothly transform into one another.

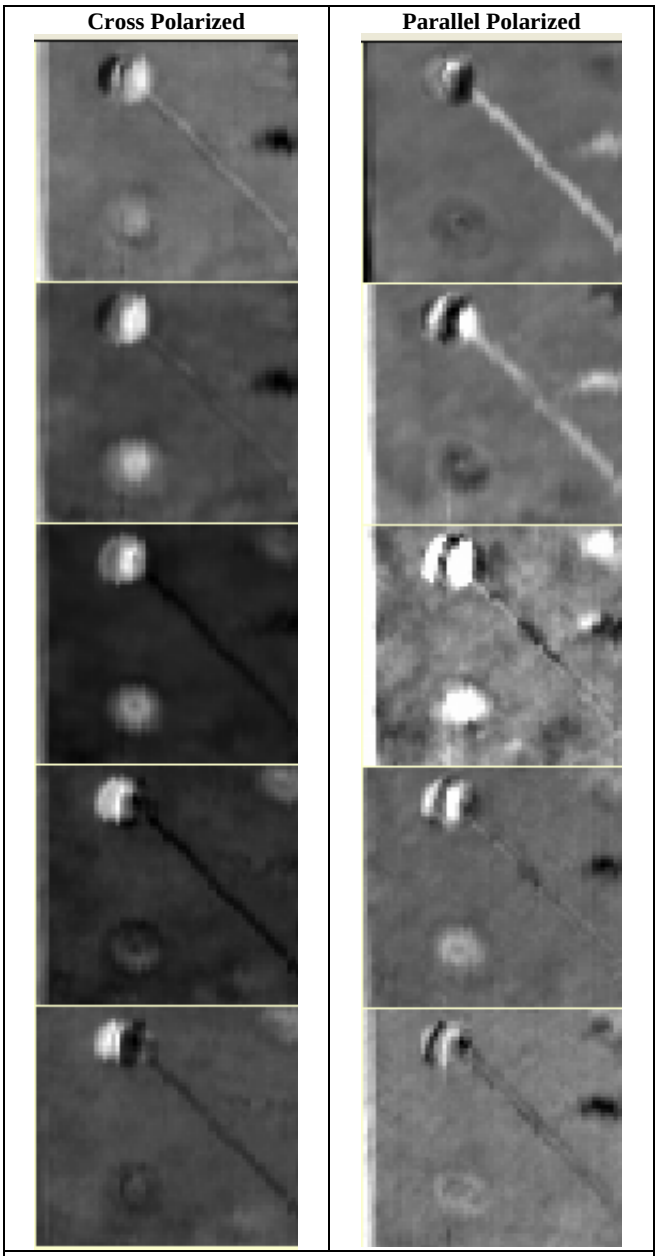

Figure 8. Ten simultaneous RASCAN images (60cm by 60cm) of landmine simulants (5 frequencies at two receiver polarizations relative to the transmitter).

Similarly, StructureScan data cannot be completely depicted by a single image as in Fig. 7, but for a different reason. Since it is impulse radar, instead of images at different frequencies, StructureScan can produce images at different time slices that effectively represent different depths (Fig. 9). The RADAN software allows the user to click through the different time slices/depths to view the 3-D block model on a computer monitor. The image in Fig. 7-c is a composite image that superimposes at each point the highest amplitude reflection from all depths at that point.

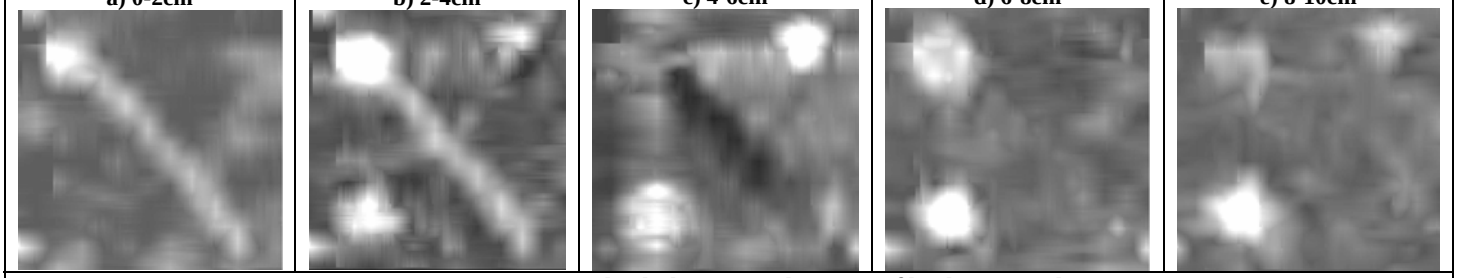

Figure 9. StructureScan depth slices (60cm by 60cm) of landmine simulants.

In a manner similar to Fig. 7 for the landmine test bed, the "best single image" results of the scanning of the clutter test bed are shown in Fig. 10. The complete RASCAN and StructureScan image sets are provided in Figs. 11 and 12 respectively.

IV. COMPARISON OF IMAGES

Inspection of the semi-coincident images for the landmine test bed (Fig. 7) show that MetalScan, RASCAN, and StructureScan all clearly delineate the metal landmine simulants. In addition, RASCAN and StructureScan delineate the wire (which appears to have shifted northwest during burial – compare Fig. 5 with Fig. 7), and the plastic case. The metal detector is not sensitive to the wire – presumably due to the (not uexpected) poor coupling between the induction coil and the long thin wire. None of the sensors provide a clear image of the PMA-2 simulant, but this seems to be due to misplacement of the scanning pad such that this important target was not encompassed. The dark apparent target on the right hand side (South) of the RASCAN images actually represents a spot where an experimenter's knee compressed the sand during backfilling. This presumably changed the porosity, and thus the bulk dielectric constant of the sand. This accident demonstrates the high sensitivity of RASCAN, and while it illustrates an advantage for detection of subtle targets, it also warns of a potential disadvantage in detection of false positives. Note that the first appearance of targets in the StructureScan depth slices (Fig. 9) is roughly correct given their burial depths, but that each target persists downward due to reverberation.

For the clutter bed, MetalScan imaged only the shallow pull tab (Fig. 10-a), and not the metal bolt, nor (again) the wire. Rascan clearly imaged all of the clutter items – including the pull tab directly on top of the deeper bolt (which can be seen as a distinct target on several frequencies/polarizations in Fig. 11). Both the MetalScan and RASCAN produced images in which apparent targets generally mimicked the actual target shapes.

The StructureScan images (Figs. 10 and 12) contain indistinct anomalies associated with the rock, bottle, and wire. An anomaly is also associated with the bolt and pull tab, but the presence of two targets is not distinguishable. On the time slices in Fig. 12, the rock, bottle and wire all appear at approximately the correct depths, while the pull tab/bolt anomaly first appears on a slice deeper than the actual pull tab depth, and persists to more than twice the depth of the bolt.

While the circular landmine simulants were accurately imaged by the impulse radar, none of the impulse radar anomalies for the elongate clutter items have shapes that closely resemble the actual targets. This may be due to an observed apparent lateral inconsistency in dielectric constant for the sand matrix of the test bed. Fig. 13 shows a raw impulse radar B-scan profile, and the same profile migrated (using Radan by GSSI) for different assumed pulse velocities. Note how the parabolic reflections on the left and right collapse to "points" at different pulse velocities. Interestingly, a linear anomaly not related to any of the buried objects cuts across the lower left corner of both the RASCAN and StructureScan images (compare, e.g., the lower left corner of the cross polarized RASCAN images in Fig. 11 to the same corner of the StructureScan time slice in Fig. 12-e). This may be further evidence of lateral changes in dielectric constant in the test bed itself despite the nominal and intended uniformity of the sand matrix.

The overall performance of the three sensors, in this specific set of tests, is summarized in Table 2.

Table 2. Performance of Sensors In This Study

	MetalScan	RASCAN	StructureScan
Observed Parameters (this study)			
Target detection	Good for shallow metal	Good for all targets	Good for Landmine simulants, fair for clutter
Target discrimination	Good for shallow metal	Good for all targets	Good for Landmine simulants, poor for clutter
Target depth measurement:	None	None	Accurate
Plan-view imaging of detected targets:	Accurate	Accurate	Accurate for landmine simulants, inaccurate for clutter

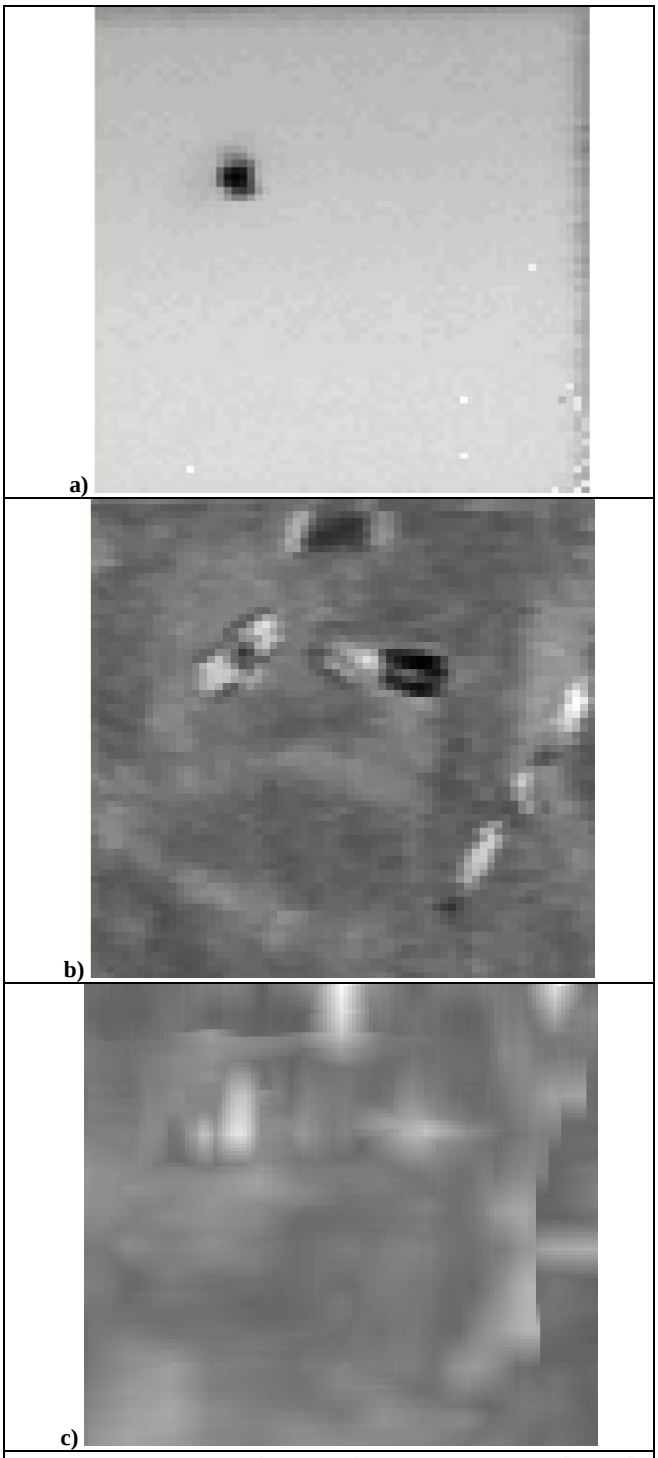

Figure 10. Semi-coincident MetalScan (a), RASCAN (b), and StructureScan (c) images (60cm by 60cm) of clutter items.

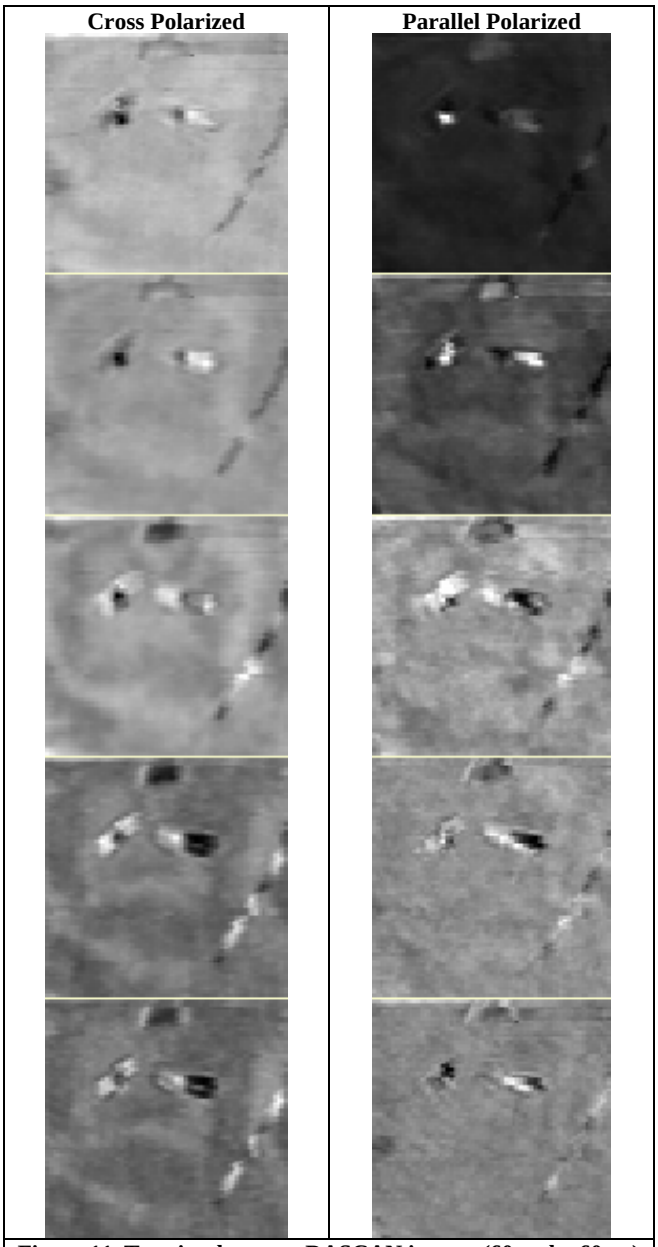

Figure 11. Ten simultaneous RASCAN images (60cm by 60cm) of clutter items (5 frequencies at two receiver polarizations relative to the transmitter).

Figure 12. StructureScan depth slices (60cm by 60cm) of clutter items.

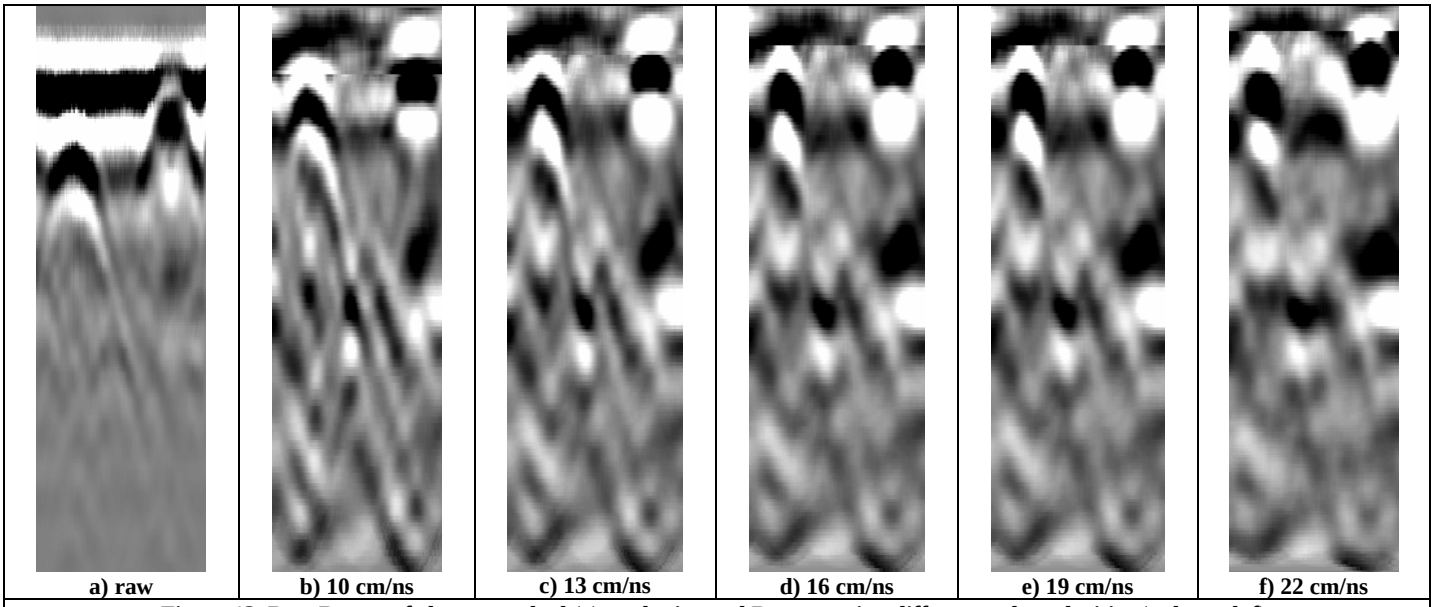

Figure 13. Raw B-scan of clutter test bed (a), and migrated B-scans using different pulse velocities (a through f).

As described above, all three sensors performed well for detecting landmine simulants. The exception is the RTV-filled PMA-2, which despite being perhaps the most interesting target, inadvertently fell outside the scanning grid. In addition, the circular footprints of these targets are apparent to all sensors.

The MetalScan was sensitive to only the shallowest metal clutter (the pull tab), but provided a reasonably accurate size, and to a lesser degree, shape for this target. The effective depth of this sensor could be easily increased based on adjustment of the operating frequency, coil diameter, or windings. The insensitivity of MetalScan to the wires is a fundamental limitation for targets of this configuration.

RASCAN detected all of the clutter items and provided accurate plan-view images. StructureScan detected the clutter items, but did not provide distinctive plan-view shapes. Of the sensors tested, only StructureScan provided target depth information, and it proved to be reasonably accurate for all targets except the superimposed pull tab and bolt.

In summary, for a multi-sensor system for landmine detection and discrimination that conforms to the criteria listed in the Introduction;

1. Holographic radar or metal detector are favored in terms of cost.
2. All three sensors can be built into platforms that are easy to transport.
3. Holographic radar and metal detector are well-suited off-the-shelf for easy operation and transportation, while impulse radar can certainly be designed for easy use. However, holographic radar does not require any assumption or determination of dielectric constant to provide accurate images, and inferred lateral changes in dielectric do not strongly affect the apparent footprint of targets.
4. All three sensors can be built into rapidly deployable platforms.
5. Impulse and holographic radar are best suited for high probability of detection for targets of arbitrary construction, however simultaneous use of the metal detector increases this probability.
6. As a single sensor, holographic radar may provide the

lowest false alarm rate due to the clear differences between landmine and clutter images – even including the phantom target represented by the knee print in Fig. 8. However, simultaneous use of additional sensors would undoubtedly lower the false alarm rate.

7. The clear images of holographic radar suggest the possibility of landmine type identification, especially when combined with a metal detector, but the current testing is insufficient to make confident claims.
8. This testing was performed in a carefully controlled test bed, so performance under actual field conditions cannot be addressed. However, the dramatic appearance of a subtle knee imprint on the holographic radar images, suggests that holographic radar may be particularly susceptible to variable site conditions.

Finally, these eight criteria do not comprehend the ability of impulse radar to determine the depth of targets. While this is certainly a distinct advantage for many subsurface detection applications, it may not offer much advantage in landmine detection where targets are typically shallow enough that depth could easily be determined by probing with a sapper spike if desired. In addition, work is proceeding on reconstruction of holograms from the microwave interference pattern [17, 18], and this could lead to retrieval of depth information even from holographic radar.

V. CONCEPTUAL DATA FUSION

It is widely proposed that fusion of data from different sensors would improve probability of detection and lower the rate of false alarms [7], [19], [20], and this is supported by some controlled testing [10], [11], [12], [13]. The data sets from the three sensors in this study should be fusable – particularly the scalar and pseudo-coincident MetalScan and RASCAN data (which are truly coincident in a MiRASCAN or ISTC type device as in Fig. 1), and can thus be readily subjected to pixel-level fusion.

Crude examples of possible pixel-level fusion schemes, as done in post-processing for the data sets in this study, are shown in Fig. 14. In each of these, the metal detector data have been converted to a binary (yes/no) image by converting each pixel to a value of -1 or 1 depending on whether the original metal detector response falls within the upper three or lower one quartile (of values for the full image) respectively. These new values are multiplied by the original pixel values for the holographic radar images in Fig. 14-a. In Fig. 14-b, the binary "metal factor" data are multiplied by the magnitude of the total gradient at each pixel of the holographic image. This type of procedure would require near-real-time fusion, but could be programmed quite easily. This procedure produces colored images in shades of yellow to red for metal targets, and green to blue for non-metal targets. The insensitivity of the metal detector to wires mis-identifies the wire placed in the test bed as non-metallic. Along the LHS of the images, there is another wire which is embedded in the data collection pad, which is also not registered by the metal detector.

Note that if the hologram can be reconstructed from the radar interference patterns, more sophisticated data fusion may not be necessary since reconstruction could produce an accurate visual image of the target, with its composition indicated by the metal detector.

Note also that a single image (3.9 GHz, parallel channel) provides a better image than a crude attempts to combine all ten holographic images as depicted in Fig. 14-c, where the rms value of the gradient for all images is depicted. In this image, the non-metal landmine simulant appears more clearly (which would translate to higher probability of detection), and the knee print on the left hand side is faint (which would translate to a possible lower false alarm rate). Since images from polarizations and frequency combinations might provide the better image for other targets or settings, more work is required to develop methods for more effectively combining and/or selecting individual radar images for landmine identification.

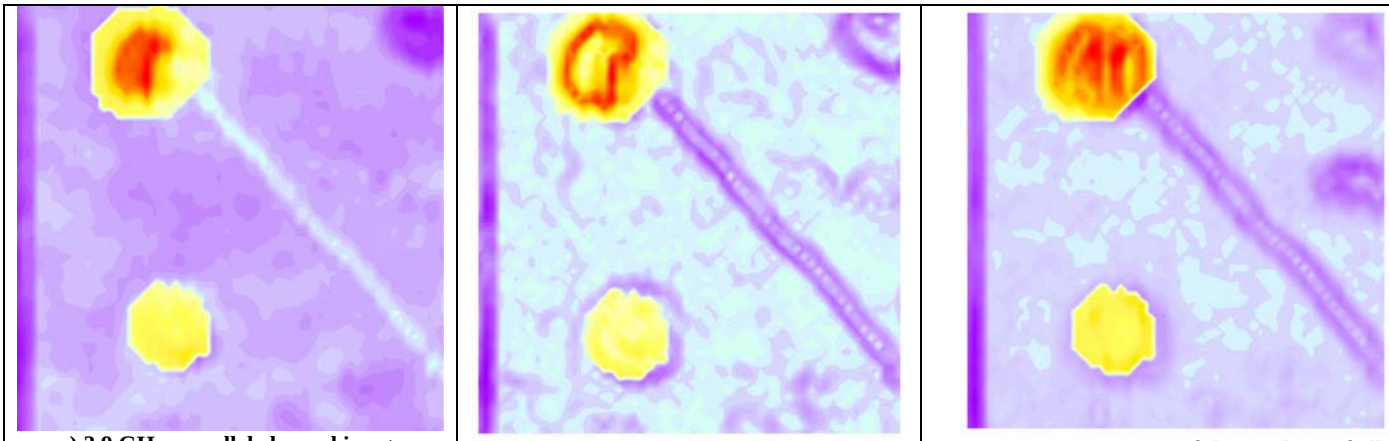

a) 3.9 GHz, parallel channel image

b) 3.9 GHz, parallel channel image gradient

c) Root mean square of the gradient of all frequencies and polarizations

Figure 14. Examples of possible data fusion schemes

In addition, work has begun on automated target recognition algorithms that could be applied to the holographic and metal detector images. The difficult task of fusion of the time-series impulse radar data with the scalar holographic and metal detector data are left as possible future work, and could be rendered unnecessary if holographic reconstruction can be accomplished.

ACKNOWLEDGMENTS

Funding for this work was provided by NATO Project CBP.NR.NRCLG.982520.

REFERENCES

[1] Kohn, G. C., *Dictionary of Wars*, Facts on File, New York, NY (1986)

[2] Mines Action Canada, *Landmine Monitor Report 2006: Toward a Mine-Free World*, International Campaign to Ban landmines, Ottawa, Canada (2006)

[3] Zhukov, S., "Experience of demining in local conflicts," *Foreign Military Review*, Moscow, no. 6, pp. 14-19 (1998).

[4] Banks, E., *Brassey's Essential Guide to Anti-Personnel Landmines; Recognising and Disarming*. Brassey's, London, UK (1997).

[5] Joynt, V.P., "Mobile metal detection: a field perspective", *Proceedings of the Second International Conference on the Detection of Abandoned Land Mines*, Edinburgh, UK, pp. 14-15 (1998).Eudem, Projects Index, http://www.eudem.vub.ac.be/projects/ (2008).Macdonald, J., et al., *Alternatives for Landmine Detection*, RAND, Santa Monica, CA (2003).

[8] Harmon, R.S., et al. (eds.), *Detection and Remediation Technologies for Mines and Minelike Targets X*, Proceedings of the SPIE, vol. 5794 (2005).

[9] Daniels, D.J., *Ground Penetrating Radar*, 2nd edition, The Institution of Electrical Engineers, London, UK (2004).

[10] Geo-Centers, *Energy focusing Ground Penetrating Radar (EFGPR) Overview*, http://www.geo-centers.com/products/EFGPR-Overview-1-03.pdf (2003).

[11] Doheny, R.C., *Handheld Standoff Mine Detection System (HSTAMIDS) Program and Operations Update*, http://www.mineaction.org/downloads/1/1FinalHSTAMIDS.ppt#1 (2007).

[12] Daniels, D. J., et al. "MINEHOUND production development", *Proceedings of the SPIE*, vol. 5794, pp. 488-494 (2005).

[13] Chignell, R.J., *Lotus – a major technology milestone or de-mining*, http://www.eudem.vub.ac.be/files/lotus_ver.pdf (2002)

[14] Ivashov S.I., et al., "Remote Control Mine Detection System with GPR and Metal Detector", *Proceedings of the Eight International Conference on Ground Penetrating Radar*, Queensland, Australia, pp. 36-39 (2000).

[15] Ivashov, S.I., et al., " Holographic Subsurface Radar Technique and its Applications", *Proceedings of the 12th International Coinference on Ground Penetrating Radar*, Birmingham, UK (2008).

[16] Bruschini, C., et al., "Ground penetrating radar and imaging metal detector for antipersonnel mine detection", *Journal of Applied Geophysics* vol. 40, pp. 59-71 (1998).

[17] Chapursky, V.V., et al., "Microwave Hologram Reconstruction for the RASCAN Type Subsurface Radar, *Proceedings of the Ninth International Conference on Ground Penetrating Radar*, Santa Barbara, California USA, pp. 520-526 (2002).

[18] Pasmurov, A-Y. et al., "*Radar Imaging and Holography*", Institution of Electrical Engineers, London (2005).

[19] Bruschini, C., et al. *EUDEM: The EU in humanitarian DEMining Final Report*, http://www.eudem.vub.ac.be/publications/Files/eudemfinal.pdf (1999)

[20] Windsor C.G. et al., "Combining results from different mine detection techniques", *Euroconference MINE'99*, Firenze, Italy, pp. 91-96 (1999).